Oxygen Reduction Hot Paper

How to cite: *Angew. Chem. Int. Ed.* **2023**, *62*, e202214074
International Edition: doi.org/10.1002/anie.202214074
German Edition: doi.org/10.1002/ange.202214074

Evidence of Sulfur Non-Innocence in $[Co^{II}(dithiacyclam)]^{2+}$-Mediated Catalytic Oxygen Reduction Reactions

Beatrice Battistella, Linda Iffland-Mühlhaus, Maximillian Schütze, Beatrice Cula, Uwe Kuhlmann, Holger Dau, Peter Hildebrandt, Thomas Lohmiller, Stefan Mebs, Ulf-Peter Apfel, and Kallol Ray**

Abstract: In many metalloenzymes, sulfur-containing ligands participate in catalytic processes, mainly via the involvement in electron transfer reactions. In a biomimetic approach, we now demonstrate the implication of S-ligation in cobalt mediated oxygen reduction reactions (ORR). A comparative study between the catalytic ORR capabilities of the four-nitrogen bound $[Co(cyclam)]^{2+}$ (**1**; cyclam = 1,5,8,11-tetraaza-cyclotetradecane) and the S-containing analog $[Co(S_2N_2\text{-cyclam})]^{2+}$ (**2**; S_2N_2-cyclam = 1,8-dithia-5,11-diaza-cyclotetradecane) reveals improved catalytic performance once the chalcogen is introduced in the Co coordination sphere. Trapping and characterization of the intermediates formed upon dioxygen activation at the Co^{II} centers in **1** and **2** point to the involvement of sulfur in the O_2 reduction process as the key for the improved catalytic ORR capabilities of **2**.

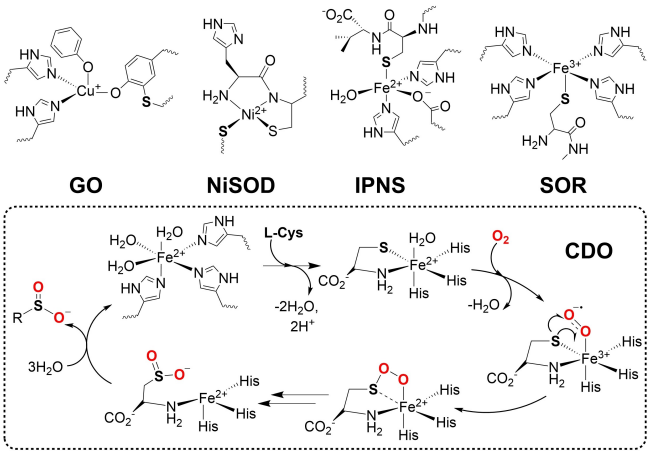

Scheme 1. Active sites of various enzymes containing sulfur in the first or second coordination spheres; the proposed mechanism of cysteine dioxygenase (CDO) is highlighted in the inset.

Introduction

Metal-sulfur centers are widespread in biology and are involved in promoting a number of critical biological processes.[1,2] For example the active site of galactose oxidase (GO)[3–5] is composed of a copper center attached to a post-translationally generated Tyrosine-Cysteine (Tyr-Cys) ligand, which facilitates the formation of the catalytically relevant oxidized state at a low potential (Scheme 1). Similarly, in Ni-dependent superoxide reductase (NiSOD) the Cys residues are proposed to be crucial for the efficient degradation of superoxide ion by stabilizing a square planar geometry in the reduced form of NiSOD and tuning the Ni^{II}/Ni^{III} redox potential.[6,7] Furthermore, the presence of a Cys residue in Isopenicillin N-synthase (IPNS)[8,9] makes this enzyme a special class of αKG-dependent Fe^{II}/O_2 activating enzymes, which exhibits oxidase rather than the usual oxygenase activity. In addition, the active site of superoxide reductases (SORs)[10–12] containing a redox-active Fe^{II} ion ligated by four

[*] M.Sc. B. Battistella, B.Sc. M. Schütze, Dr. B. Cula, Dr. T. Lohmiller, Prof. Dr. K. Ray
Institut für Chemie, Humboldt-Universität zu Berlin
Brook-Taylor-Straße 2, 12489 Berlin (Germany)
E-mail: kallol.ray@chemie.hu-berlin.de

M.Sc. L. Iffland-Mühlhaus, Prof. Dr. U.-P. Apfel
Faculty of Chemistry and Biochemistry, Ruhr-Universität Bochum
Universitätsstraße 150, 44780 Bochum (Germany)
E-mail: ulf.apfel@rub.de

Dr. U. Kuhlmann, Prof. Dr. P. Hildebrandt
Institut für Chemie, Fakultät II, Technische Universität Berlin
Straße des 17. Juni 135, 10623 Berlin (Germany)

Prof. Dr. H. Dau, Dr. S. Mebs
Institut für Physik, Freie Universität zu Berlin
Arnimallee 14, 14195 Berlin (Germany)

Dr. T. Lohmiller
EPR4Energy Joint Lab, Department Spins in Energy Conversion and Quantum Information Science, Helmholtz Zentrum Berlin für Materialien und Energie GmbH
Albert-Einstein-Str. 16, 12489 Berlin (Germany)

Prof. Dr. U.-P. Apfel
Department for Electrosynthesis, Fraunhofer Institute for Environmental, Safety and Energy Technology UMSICHT
Osterfelder Str. 3, 46047 Oberhausen (Germany)

equatorial histidines and an axial Cys ligand, enables the selective transformation of superoxides to hydrogen peroxide, in contrast to Fe-containing superoxide dismutases,[13,14] which lack the Cys ligand and disproportionate superoxide to afford both hydrogen peroxide and dioxygen. In cysteine dioxygenase (CDO) the Fe-coordinated thiolate of Cys is proposed to be directly involved in dioxygen activation, by the formation of a transient (Fe^{II}–O_2–S–Cys) moiety, followed by further oxidation to yield the corresponding sulfonate (Scheme 1).[15,16]

Understanding the reason for Nature's choice of employing cysteinate and thioether residues to promote specific biological functions in metalloenzymes requires a comprehensive investigation of the influence of thiolate or thioether ligands on the electronic, magnetic, and reactivity properties of first-row transition metal ions. Based on detailed spectroscopic and theoretical studies the unique reactivities of the metal-sulfur sites in oxidases and oxygenases has been attributed to the stabilization of reactive intermediates formed by the unfavorable one-electron reduction of O_2, by delocalization of the redox active orbitals onto the thioether or cysteinate sulfur atoms.[4,13] Consistent with this explanation the presence of sulfur ligation is shown to induce novel dioxygen reactivity in bioinspired iron,[13,17–20] copper,[21–23] manganese[24–26] and cobalt[26] complexes, which led to the stabilization of well-defined metal-oxygen intermediates. However, there is little evidence to support the redox non-innocence of sulfur in these research works.

In previous studies, we demonstrated that the replacement of the opposing nitrogen atoms in 1,4,8,11-tetraazacyclotetradecane (cyclam) with two sulfur atoms in 1,8-dithia-4,11-diaza-cyclotetradecane (dithiacyclam) enabled the electrochemical reduction of protons and CO_2 by the corresponding Ni^{II} [27] and Co^{II} [28] complexes at more positive potentials. The lack of any isolable reactive intermediates in these reactions, however, prevented us from obtaining detailed mechanistic insights into the role of sulfur in enabling the $[M^{II}(dithiacyclam)(CH_3CN)_2]^{2+}$ (M = Co, Ni) mediated CO_2 and H^+ reductions at low overpotentials. In the present study, we show that the $[Co^{II}(dithiacyclam)(CH_3CN)_2]^{2+}$ (**2**) complex (Scheme 2) is also an excellent catalyst for the oxygen reduction reaction (ORR) which is crucial to diverse processes ranging from biological respiration[29] and fuel cells[30] to the selective oxidation of organic molecules.[31] Most importantly, **2** performs the $2e^-/2H^+$ reduction of dioxygen to H_2O_2 with high selectivity at an effective overpotential as low as 66 mV, in contrast to the significantly higher value (419 mV) determined for $[Co^{II}(cyclam)(CH_3CN)_2]^{2+}$ (**1**; Scheme 2) under analogous conditions. The difference in the ORR capabilities of $[Co^{II}(dithiacyclam)(CH_3CN)_2]^{2+}$, containing a S_2N_2 macrocyclic ligand, and $[Co^{II}(cyclam)(CH_3CN)_2]^{2+}$, based on the popular N_4-cyclam ligand, is demonstrated to originate from distinct Co–O_2 intermediates formed upon dioxygen activation in the two cases. Although, diverse complexes have been previously reported in the literature[30,32] that exhibit high rates and/or high selectivity for O_2 reductions to H_2O or H_2O_2, a particular challenge is the identification of molecular catalysts that operate with low effective overpotentials. The mechanistic insights obtained in this study should, therefore, provide useful and broadly applicable principles for future design of more efficient ORR catalysts working at low overpotentials, by making use of the redox non-innocence of sulfur containing ligands.

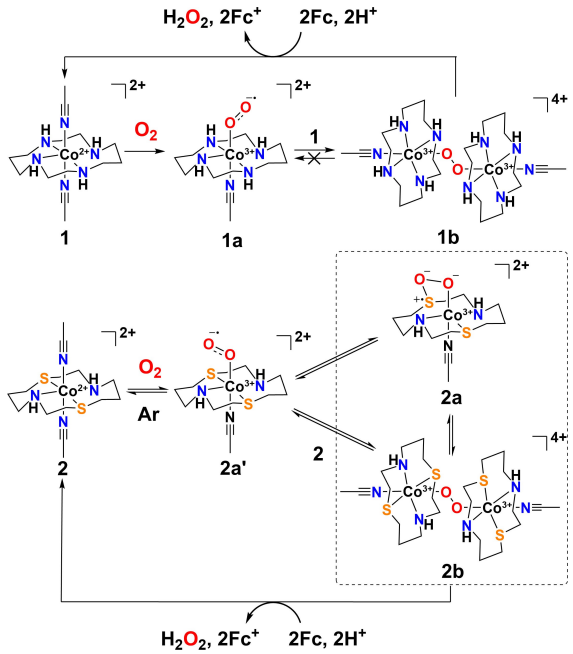

Scheme 2. Schematic structures showing the distinct reaction intermediates formed in the reactions of **1** and **2** with O_2.

Results and Discussion

Combining the tetradentate cyclam and dithiacyclam ligands with $Co(ClO_4)_2$ in CH_3CN yielded the previously characterized[28] $[Co^{II}(cyclam)(CH_3CN)_2](ClO_4)_2$ (**1**) and $[Co^{II}(dithiacyclam)(CH_3CN)_2](ClO_4)_2$ (**2**), respectively. The molecular structures of **1** and **2** have been reported previously, and display a six coordinate geometry with axially bound CH_3CN ligands in both cases (Scheme 2). The S_2N_2 donor atoms of dithiacyclam in **2** and N_4-donor atoms in **1** occupy the equatorial coordination sites. The X-band EPR spectra in frozen CH_3CN solutions at 13 K show an axial signal ($g_\perp = 2.27$, $g_\parallel = 1.94$) for **1** and a nearly isotropic signal at $g_{average} = 2.19$ for **2**, confirming the $S = 1/2$ spin state in both cases (Figure S1a, b). Whereas the exchange of the axial ligands has no significant effect on the coordination sphere or the spin-state of the central Co^{II} ion in **1**, replacement of the CH_3CN ligands with methanol, acetone or trifluoroacetate ligands leads to an altered geometry with axial sulfur donor atoms and stabilization of the $S = 3/2$ ground state in $[Co^{II}(dithiacyclam)(X)_2]^{Y+}$ (Figure S1c; X = MeOH, CH_3COCH_3, Y = 2+ or X = TFA^-, Y = 0, Tables S7, S8, ***2-cis***). Cyclovoltammetric studies on **1** and **2** in CH_3CN reveal a quasi-reversible oxidation wave corresponding to a $Co^{III/II}$ couple (Figure S2). A large anodic shift of the $Co^{III/II}$ potential is observed for **2** in acetone (Figure S2), likely because of the gradual replacement of the CH_3CN ligands with acetone to

form **2-*cis***, as also evident from X-band EPR studies (Figure S1c).

The ORR capability of **1** and **2** was further investigated by UV/Vis spectroscopy. Both **1** and **2** performed catalytic ORR even in presence of a weak electron donor like ferrocene (Fc) using trifluoroacetic acid (TFA) as a proton source. Catalytic ORR was monitored by a rise in absorbance at 619 nm, which is attributable to the formation of a ferrocenium (Fc^+) cation.[33] Iodometric titration[34] (Figure 1, insets) of the final reaction mixture shows that H_2O_2 is formed with high selectivity in both cases (100 % yield of H_2O_2 for **2** and 62 % for **1** based on the maximum expected yield of H_2O_2 considering $2e^-$ reduction of O_2), according to the mechanism reported in Equation (1). Notably, in absence of **1** and **2**, the formation of Fc^+ could not be detected by UV/Vis spectroscopy and no H_2O_2 was shown to be formed under the employed experimental conditions (Figure S3). The ORR capabilities of **1** and **2** were then compared under a uniform set of conditions in acetone and CH_3CN using decamethylferrocene (Fc*) as an alternative chemical reductant.[32,35,36] O_2 and iodometric titrations[34] and ^{1}H NMR[37] (Figures S4–S6) studies confirmed the two-electron reduction of O_2 to H_2O_2 with high selectivity in both cases. Turnover frequencies (TOFs) for the conversion of O_2 to H_2O_2 were determined from the initial rates of decamethylferrocenium ion (Fc^{*+}) formation by UV/Visible spectroscopy under buffered conditions (TFA and NaTFA = sodium trifluoroacetate, 10 mM each) (Figures S7, S8).[32,38,39] The collected data were further analyzed to assess the effective overpotential (η_{eff}) for the reactions (Scheme S1), which is defined as the difference between the thermodynamic potential for O_2 reduction to hydrogen peroxide ($E(O_2/H_2O_2)$) and the $E_{1/2}(Co^{III/II})$ values under buffer conditions [Eq. (2); Figures S9–S11]. Following the reported methodology for the determination of the overpotential under non-aqueous conditions, E_{O_2/H_2O_2} could be determined in the solvents of use by open-circuit potential (OCP) measurements (E_{H^+/H_2} determination, Figures S12, S13, see Supporting Information for details).[32,38,39] The thermodynamic analysis yielded an η_{eff} value of 66 mV for **2** in acetone, which is the lowest overpotential that has been measured (typical range 150–550 mV) for the cobalt mediated catalytic reduction of O_2 to H_2O_2 under buffer conditions.[32] Most importantly, complex **1** showed a significantly lower TOF and higher overpotential (η_{eff} = 419 mV in acetone, Table S1) under similar conditions, thereby demonstrating the beneficial influence of sulfur-based ligands on O_2 reduction processes.

$$O_2 + 2H^+ + 2e^- \rightarrow H_2O_2 \qquad E^\circ = 0.68\ \text{V vs. NHE} \tag{1}$$

$$\eta_{eff} = E(O_2/H_2O_2) - E_{1/2}(Co^{III/II}) \tag{2}$$

In order to elucidate the catalytic mechanism and to explain the differences in the O_2/H_2O_2 η_{eff} for **1** and **2**, we examined the reactions of **1** and **2** with O_2 (in the absence of TFA/NaTFA and electron donors) to detect the formation of any cobalt-dioxygen intermediates. Treatment of an acetone solution of **1** with O_2 at −70 °C resulted in the formation of a metastable ($t_{1/2}$ at −55 °C = 2.5 h) yellow species **1a** with absorption maxima λ_{max} (ε_{max}) at 330 nm (1900 $M^{-1}\,cm^{-1}$) and 455 nm (220 $M^{-1}\,cm^{-1}$) (Figure 2a). Such features are in line with what has been reported for Co^{III}-superoxo moieties, which often present intense absorption in the range 330–380 nm and a less intense feature in the range 420–480 nm.[40,49] The conversion of **1** to **1a** is associated with the

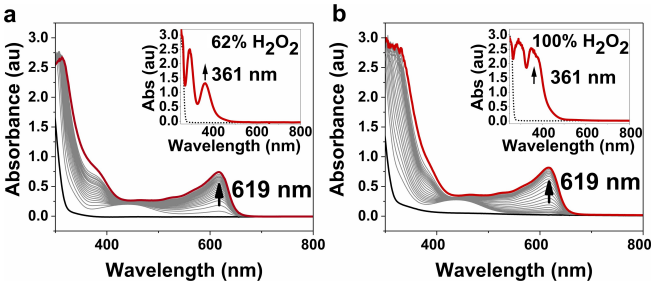

Figure 1. UV/Vis spectral changes in the two-electron reduction of O_2 by Fc (3 mM) with 0.1 mM **1** (a) and **2** (b) in presence of 10 mM TFA in O_2-saturated (12.1 mM) CH_3CN (total volume = 2.0 mL) at 25 °C; inset: iodometric titration performed on an aliquot (0.1 mL) of the final reaction mixture confirmed H_2O_2 formation. The yield is based on the maximum possible yield of H_2O_2 (0.075 mM) according to Equation 1. See also Figures S4, S5.

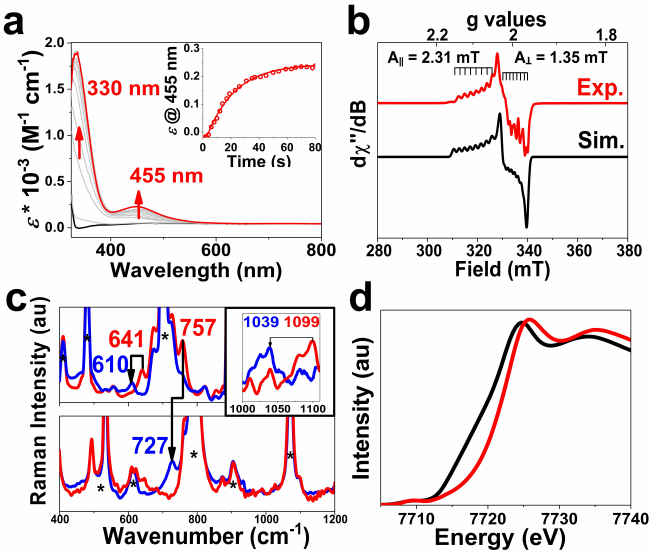

Figure 2. a) UV/Vis spectral changes associated with the reaction of **1** with O_2 at −70 °C in acetone. The time trace of the development of the 455 nm band is shown in the inset. b) X-band EPR spectrum (red) of a **1**/O_2 mixture in acetone (1 mM) at 13 K and the corresponding simulated spectrum (black). Experimental details: perpendicular mode, ca. 9.35 GHz, 1 mW power; simulation parameters: $g_{||} = 2.10$, $g_{\perp} = 2.00$, $A_{||} = 2.31$ mT, $A_{\perp} = 1.35$ mT. c) rRaman spectra of a 8 mM **1**/O_2 mixture in acetone-d_6 (top) and acetone (bottom) at −70 °C upon excitation with 406 nm laser; the corresponding spectrum in CH_2Cl_2 is shown as an inset; the spectra in presence of $^{16}O_2$ are shown in red and $^{18}O_2$ in blue. Asterisks indicate the solvent bands. d) Co *K*-edge XAS spectra of **1** (black) and of a **1**/O_2 mixture (red) in frozen acetone solutions at 20 K.

appearance of a new axial EPR spectrum with $g_{\|}=2.10$, and $g_{\perp}=2.00$ (Figure 2b) and well resolved ^{59}Co hyperfine features with couplings $A_{\|}=2.31$ mT, and $A_{\perp}=1.35$ mT. These EPR parameters resemble those of $Co^{III}(O_2^{\bullet-})$ superoxo species reported previously.[40–43] Quantification of the Co^{II} and Co^{III}-$(O_2^{\bullet-})$ EPR spectra in acetone reveals that only approximately 25 % of the total number of spins present in the initial anaerobic Co^{II} sample are converted to the $Co^{III}(O_2^{\bullet-})$ intermediate (Figure S14). The low quantity of the $Co^{III}(O_2^{\bullet-})$ signal may be rationalized by the simultaneous formation of a peroxide-bridged Co^{III} dimer **1b** (Scheme 2, $Co:O_2=2:1$) which is EPR-silent under the employed experimental conditions (X-band, perpendicular mode). Such dimeric species have been observed with other Co complexes bearing tetradentate ligands[41,44] and have also been suggested as a plausible intermediate during the complex **1** mediated electrocatalytic ORR process.[45–48] The resonance Raman (rR) spectra of the reaction mixture of **1** and O_2 in acetone and acetone-d_6 (Figure 2c) display two isotopically sensitive vibrational bands at 757 and 641 cm^{-1}, which in $^{18}O_2$ prepared samples are downshifted to 727 and 610 cm^{-1}, respectively. The 757 cm^{-1} band with an isotopic shift of 30 cm^{-1} (calculated shift $^{16/18}\Delta_{calc.}=43$ cm^{-1}) is assigned to the O–O stretching mode of a peroxo ligand in **1b**, and the 641 cm^{-1} band ($^{16/18}\Delta_{exp.}=31$ cm^{-1}, $^{16/18}\Delta_{calc.}=29$ cm^{-1}) is consistent with a Co–O stretching mode. Solvent bands mask the region between 1000–1150 cm^{-1} in acetone and acetone-d_6, preventing the observation of the O–O stretching mode from the $Co^{III}(O_2^{\bullet-})$ species **1a** under these conditions. Changing the solvent to dichloromethane allowed the isolation of an additional ^{18}O–isotope sensitive vibrational band at 1099 cm^{-1} with an ^{18}O-isotopic shift of 60 cm^{-1} (Figures 2c inset, S15), consistent with its assignment to the O–O stretching mode of the superoxo ligand in **1a**. Notably, no Co–O vibration corresponding to **1a** could be observed, which is presumably masked by the solvent signal (Figure 2c) or by the intense Co–O vibration band of **1b** (at 636 cm^{-1}), which is formed in much higher yield relative to **1a**. The DFT calculated O–O and Co–O vibrational modes of **1a** and **1b** are in reasonable agreement with the experiment (Table S2). Furthermore, topological analysis of the electron density (AIM) and non-covalent interaction index (NCI) on the DFT computed structure of **1a** (Figure S16) show that two of the four –NH hydrogens of the cyclam macrocycle point towards the superoxo ligand and are located at only 2.1 Å distance from the distal oxygen atom of the *end-on* bound $(O_2)^{\bullet-}$ moiety. The negative charge on $(O_2)^{\bullet-}$ promotes the hydrogen bonding interaction and electron density transfer from the N–H groups to $(O_2)^{\bullet-}$, stabilizing the superoxo species by conferring it a higher peroxo-character. This results in a O–O stretching frequency (calculated: 1078 cm^{-1}; experimental: 1099 cm^{-1}), which is significantly lower compared to the previously reported $Co^{III}(O_2^{\bullet-})$ species (1153–1123 cm^{-1}).[49,50] In order to probe the oxidation state of cobalt in **1a/1b**, X-ray absorption spectroscopic (XAS) studies at the Co *K*-edge were performed. Figure 2d depicts a comparison of the normalized Co *K*-edge XAS spectra of the **1**/O_2 reaction mixture with the Co^{II} precursor complex **1**. A blue shift of ca. 2.5 eV in edge energy from **1** (7718.8 eV) to **1a/1b** (7721.3 eV) and comparison to cobalt standards of known oxidation states agree with the higher oxidation state of cobalt in **1a/1b** (Co^{III}) relative to **1** (Co^{II}) (Figure S17). The presence of a Co–O_2 unit in **1a/1b** was confirmed by EXAFS analysis, which yielded the best-fit plot (Figure S17, Table S3) with an O/N scatterer at 1.86 Å (assigned to the Co–O scatterer) and a further shell of five O/N scatterers at 1.96 Å (corresponding to the N-donors of cyclam and CH_3CN). Fine structural details are visible in the EXAFS wave, which were calculated for the DFT models of **1a/1b** and compared to the experimental spectra. The best fit corresponds to the presence of a mixture of **1a/1b** in the O_2 saturated solution of **1** (Figure S18, Table S4), consistent with EPR studies.

Complex **2** reacts with O_2 in CH_3CN or acetone at −30 °C to form a deep red species **2a/2b**, whose absorption bands at $\lambda_{max}=495$ and 695 nm ($\varepsilon_{max}=1550$ and 350 $M^{-1}cm^{-1}$, respectively; $t_{1/2}$ at 10 °C = 250 s; Figure 3a) are clearly distinct from the absorption spectrum of **1a/1b** and similar to what has been reported for several Co^{III}-peroxo moieties, which generally exhibit absorption features in the range from 500 nm to 700 nm.[50] Furthermore, in contrast to the irreversible conversion of **1** to **1a/1b**, the formation of **2a/2b** is reversible. Flushing with argon for 30 seconds led to the decay of **2a/2b**, which could then be regenerated upon

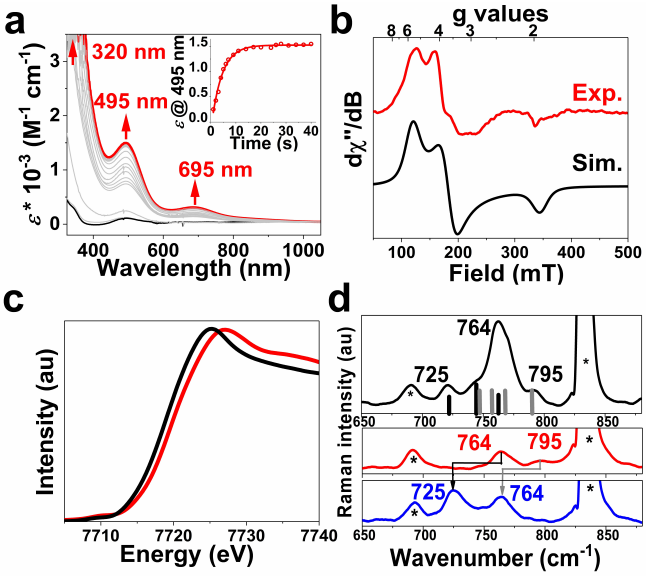

Figure 3. a) UV/Vis spectral changes associated with the reaction of **2** with dioxygen at −30 °C in CH_3CN. The time trace of the development of the 495 nm band is shown in the inset. b) X-band EPR spectrum (red) of **2**/O_2 mixture in CH_3CN (1 mM) at 13 K and the corresponding simulated spectrum (black). Experimental details: perpendicular mode, 9.35 GHz, 1 mW power; simulation parameters: $g^{eff}_x=5.59$, $g^{eff}_y=3.65$, $g^{eff}_z=1.94$). c) Co *K*-edge XAS spectra of **2** (black) and of a **2**/O_2 mixture (red) in frozen CH_3CN solutions at 20 K. d) rRaman spectra of a 8 mM **2**/O_2 mixture in CD_3CN at −30 °C upon excitation with 514 nm; the red, blue and black traces correspond to the data recorded in presence of $^{16}O_2$, $^{18}O_2$ and a statistical mixture of $^{16}O_2$:$^{16/18}O_2$:$^{18}O_2$ (1:2:1 ratio), respectively. The DFT calculated vibrational modes for **2a** (grey) and **2b** (black) in presence of a statistical mixture of $^{16}O_2$:$^{16/18}O_2$:$^{18}O_2$ (1:2:1 ratio) are shown by the bars. Asterisks indicate the solvent bands.

addition of O_2 (Figure S19). The EPR spectrum of the reaction product of **2** with O_2 exhibits a rhombic signal with $g^{eff}{}_x = 5.59$, $g^{eff}{}_y = 3.65$ and $g^{eff}{}_z = 1.94$, which corresponds to 50 % of the total number of cobalt spins (Figures 3b, S20). Its significant anisotropy evidences a $S > 1/2$ ground state, which is attributed to the mononuclear Co–O_2 adduct **2a** (Scheme 2), the ground total spin state of which is identified as 3/2 rather than 5/2 (see below). The remaining 50 % of cobalt is attributed to the EPR-silent peroxo-bridged dicobalt(III) species (**2b**), which is characterized by X-ray crystallography. Single crystals of the metastable intermediate (Figure 4a) were obtained by Et_2O diffusion into a CH_3CN solution of the triflate salt of **2** cooled at −25 °C and exposed to O_2. As evident from the *R*-factor (8.1 %; Table S5) and estimated standard deviations, the structure of **2b** is of high quality. The ORTEP diagram in Figure 4a shows a $[(CH_3CN)Co^{III}(dithiacyclam)]_2(\textit{trans}\text{-}\mu\text{-}1,2\text{-}O_2)(OTf)_4$ (**2b**) moiety containing an O_2 ligand bridging two cobalt ions in an *end-on* trans configuration. Each Co ion is ligated by two sulfur and two nitrogen atoms in the equatorial plane, and an O_2-derived oxygen and CH_3CN in the axial sites. Notably, the O–O bond length in **2b** (1.508(6) Å, Table S6) is significantly longer than the typical values (1.43–1.48 Å) determined by X-ray crystallography for metal-peroxo complexes,[24,44,51] consistent with strong reductive activation of the O–O bond. Furthermore, XRD analysis displays hydrogen bonding interactions between one of the N–H moieties in each macrocyclic ligand and the bridging peroxo moiety (N–H–O1 = 2.477 Å; N–H–O2 = 2.101 Å, Figure 4a), which presumably contributes to the elongation of the O–O bond in **2b**. Dioxygen reduction by **2** is accompanied by a 1.3 eV blue shift of the Co *K*-edge in the XANES spectrum (Figures 3c, S21; from 7718.2 eV in **2** to 7719.5 eV upon oxygenation), which is significantly smaller than the 2.5 eV blue shift observed during the oxygenation of **1**. Nevertheless, the O–O stretching mode in **2b** (ν_{O-O} ($^{16/18}\Delta_{exp}$): 764 (39) cm^{-1}) as obtained from rRaman measurements (Figure 3d) is comparable to that observed for **1b** (ν_{O-O} ($^{16/18}\Delta_{exp}$): 757 (30) cm^{-1}). Thus, although the reductive activation of the O–O bond is comparable in **1b** and **2b**, the cobalt centers are more reduced in **2b**. This may point to a significantly higher charge donation to O_2 from the S_2N_2 donor atoms in **2b** relative to that of the N_4 centers in **1b**.

The rRaman spectrum of the **2**/O_2 mixture shows an additional ^{18}O-isotope sensitive band at 795 cm^{-1}, which shifts to 764 cm^{-1} upon ^{18}O labelling. This is assigned to the O–O stretch of the Co–O–O–S motif of a mononuclear $S = 3/2$ cyclic peroxythioether $[(CH_3CN)Co^{III}(dithiacyclam\text{-}O_2^{\bullet})]^{2+}$ (**2a**) intermediate (Scheme 2) formed by the plausible attack of the initially formed Co^{III}-superoxido species (**2a′**) to one of the thioether sulfur atoms of the dithiacyclam ligand. A rRaman investigation was also done in presence of mixed isotope O_2 ("$^{16,18}O_2$") containing a statistical mixture of $^{16}O_2$:$^{16/18}O_2$:$^{18}O_2$ (1:2:1 ratio), which further confirms the presence of both **2a**/**2b** in an oxygenated solution of **2**. Since the 795 cm^{-1} mode corresponds to an O–O stretching of an asymmetric Co–O–O–S unit in **2a**, four modes are expected corresponding to the Co–^{16}O–O^{16}–S, Co–^{18}O–O^{16}–S, Co–^{16}O–O^{18}–S and Co–^{18}O–O^{18}–S moieties in 1:1:1:1 ratio (grey bars in Figure 3d). In contrast, for the symmetric Co–O–O–Co moiety in **2b**, we should expect three peaks at 764, ≈746 and 725 cm^{-1} in 1:2:1 ratio (black bars in Figure 3d). A superposition of all the above signals presumably gives rise to the complex pattern with an intense signal at ≈764 cm^{-1} and shoulders at 725, 745 and 794 cm^{-1} in the experimental spectrum (Figure 3d), which is reproduced by the optimized DFT structures (see below, Figure S22, Table S2). Thus, in contrast to the Co^{II}(cyclam) motif, which acts as a one electron donor, the Co^{II}(dithiacyclam) core involving a S_2N_2 macrocyclic ligand acts as a two-electron donor. The non-innocence of the dithiacyclam ligand is associated with the formation of a S–O bond to yield the Co–O–O–S moiety in **2a**. Furthermore, the oxidized sulfur atom stays away from the coordination sphere of cobalt, as confirmed by EXAFS analysis (Figure S21). While the EXAFS spectrum of **2** can be best fitted with two Co–S scatterers at 2.26 Å, the corresponding spectrum for an aerobic solution of **2** can be best modelled by a partial loss of S-shell contribution (1 Co–S = 2.27 Å, 0.5 Co–S = 2.44 Å), consistent with the presence of equal amount of **2a** and **2b** (Table S3), in excellent agreement with the EPR results, and the presence of only one Co–S scatterer in **2a**. Geometry optimization performed by DFT calculation on **2a** (Figure 4b) in the $S = 3/2$ state (involving an $S = 1$ Co^{III} center that is ferromagnetically coupled to $S = 1/2$ dithiacyclam-$O_2^{\bullet-}$) can nicely reproduce the EXAFS determined metrical parameters (Table S4) and fine structures (Figure S23).[52] The asymmetric O–O stretching of the Co–O–O–S core is calculated at 789 cm^{-1}, in excellent agreement with the experiment (795 cm^{-1}). However, the $^{16/18}\Delta_{calc}$ shift is calculated to be 42 cm^{-1}, in contrast to the experimentally observed $^{16/18}\Delta_{exp}$ shift of only 30 cm^{-1}. This discrepancy can be attributed to the coupling of the O–O stretching coordinate with other coordinates, which may be underestimated in the calculations, or because of intermolecular interactions, which are not considered in DFT.

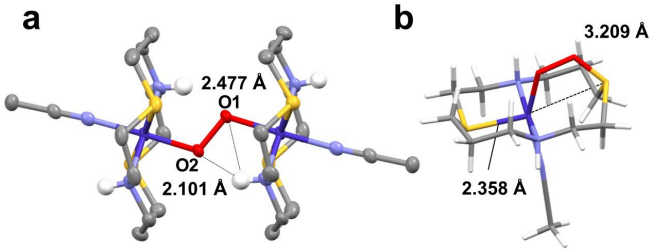

Figure 4. a) XRD determined molecular structure of $[(CH_3CN)Co^{III}(dithiacyclam)]_2(\textit{trans}\text{-}\mu\text{-}1,2\text{-}O_2)(OTf)_4$ **2b**.[53] See Table S6 for bond lengths in **2b**. H-bonding interactions are shown as dotted lines. b) DFT optimized molecular structure of **2a**, showing the loss of the Co- S(oxidized) atom ligation. The Co–S(oxidized) distance is shown as a dotted line. Color code: C grey, N blue, H white, S yellow, O red, Co purple.

Conclusion

The catalytically relevant, oxidized state of the active site [Cu^{II}–$Y^{\bullet}$–C] of galactose oxidase (GO) is composed of antiferromagnetically coupled Cu^{II} and a post-translationally generated Tyr-Cys radical cofactor [$Y^{\bullet}$–C].[4] The thioether bond of the Tyr-Cys cross-link has been shown experimentally to affect the stability, the reduction potential, and the catalytic efficiency of the GO active site. Similarly, in various non-heme iron enzymes the charge donation from the thiolate ligand is proposed to render the formation of the Fe^{III}-superoxide complex energetically favorable, driving the reaction at a single Fe center rather than the energetically more demanding bimolecular pathway.[14] Although the non-innocence of thioether and thiolate sulfur atoms is implicated in these processes, direct evidence is lacking. In a bioinspired approach we now demonstrate that the presence of thioether ligation significantly affects the ORR capability of a cobalt complex; complex **2** performs the catalytic reduction of O_2 to H_2O_2 at an effective overpotential as low as 66 mV. The high efficiency of **2** can be attributed to the formation of a cyclic peroxythioether intermediate **2a** by the attack of the initially formed Co^{III}-superoxide species at one of the thioether sulfur atoms of the dithiacyclam ligand. As suggested before in enzymatic systems,[14] this presumably opens up a low-energy mononuclear pathway for catalytic ORR processes. The formation of the novel Co–O–O–S moiety in **2a** is concluded based on combined EPR, EXAFS (loss of 1 Co–S ligation) and rRaman (O–O vibration at 795 cm^{-1}) studies, and it represents a bioinspired model of the cyclic peroxythiolate intermediate proposed in cysteine dioxygenase (Scheme 1 inset).[15,16] In the absence of sulfur ligation, the $S=1/2$ Co^{III}-superoxide species **1a** can only be reduced by an energetically more demanding dinuclear mechanism, which may contribute to the large overpotential (419 mV) required for catalytic ORR mediated by **1**. Notably, the presence of two thioether ligands does not completely shut down the dinuclear mechanism in **2**, as evident from the isolation of the crystals of **2b**. Complex **2b** features a highly activated dioxygen center with a large O–O bond length of 1.51 Å, which further signifies the strong charge donation from the dithiacyclam ligand. Whether the overpotential for O_2 reduction can be further lowered by steric inhibition of the dinuclear mechanism in **2** is now an inherent question, which will be investigated in future studies.

Acknowledgements

We thank the Deutsche Forschungsgemeinschaft (DFG; German Research Foundation) for financial support under Germany's Excellence Strategy—EXC-2033 390677874—"RESOLV" RA/2409/8-1 & AP242/5-1) and EXC-2008—390540038—"UniSysCat", as well as for support to T.L. (Project No. LO 2898/1-1). This work was further supported by the Fraunhofer Internal Programs and Einstein Center of Catalysis. Single isotope labelled gas mixture was prepared in collaboration with the group of Prof. Dr. Christian Limberg at the Humboldt-University of Berlin, for which we acknowledge Dr. Christin Herwig. We also acknowledge the Helmholtz Zentrum Berlin (HZB) for providing experimental infrastructure and allocating beamtime at beamline KMC-3 of the BESSY synchrotron. Furthermore, we thank Dr. Daniel Siegmund for the XRD molecular structure analysis performed at the Ruhr-Universität Bochum. Open Access funding enabled and organized by Projekt DEAL.

Conflict of Interest

The authors declare no conflict of interest.

Data Availability Statement

The data that support the findings of this study are available in the Supporting Information of this article.

Keywords: Cobalt · Macrocyclic Ligands · O–O Activation · Reactive Intermediates · Spectroscopy

[1] A. Krężel, W. Maret, *Chem. Rev.* **2021**, *121*, 14594–14648.
[2] J. Liu, S. Chakraborty, P. Hosseinzadeh, Y. Yu, S. Tian, I. Petrik, A. Bhagi, Y. Lu, *Chem. Rev.* **2014**, *114*, 4366–4469.
[3] J. W. Whittaker, *Chem. Rev.* **2003**, *103*, 2347–2363.
[4] D. Rokhsana, A. E. Howells, D. M. Dooley, R. K. Szilagyi, *Inorg. Chem.* **2012**, *51*, 3513–3524.
[5] S. Itoh, M. Taki, S. Fukuzumi, *Coord. Chem. Rev.* **2000**, *198*, 3–20.
[6] a) V. Pelmenschikov, P. E. M. Siegbahn, *J. Am. Chem. Soc.* **2006**, *128*, 7466–7475; b) N. Lihi, D. Kelemen, N. V. May, I. Fábián, *Inorg. Chem.* **2020**, *59*, 4772–4780.
[7] J. Shearer, *Acc. Chem. Res.* **2014**, *47*, 2332–2341.
[8] J. E. Baldwin, M. Bradley, *Chem. Rev.* **1990**, *90*, 1079–1088.
[9] P. L. Roach, I. J. Clifton, C. M. H. Hensgens, N. Shibata, C. J. Schofield, J. Hajdu, J. E. Baldwin, *Nature* **1997**, *387*, 827–830.
[10] C. Mathé, C. O. Weill, T. A. Mattioli, C. Berthomieu, C. Houée-Levin, E. Tremey, V. Nivière, *J. Biol. Chem.* **2007**, *282*, 22207–22216.
[11] E. Tremey, F. Bonnot, Y. Moreau, C. Berthomieu, A. Desbois, V. Favaudon, G. Blondin, C. Houée-Levin, V. Nivière, *JBIC J. Biol. Inorg. Chem.* **2013**, *18*, 815–830.
[12] A. Desbois, J. Valton, Y. Moreau, S. Torelli, V. Nivière, *Phys. Chem. Chem. Phys.* **2021**, *23*, 4636–4645.
[13] L. M. Brines, J. A. Kovacs, *Eur. J. Inorg. Chem.* **2007**, 29–38.
[14] a) J. A. Kovacs, L. M. Brines, *Acc. Chem. Res.* **2007**, *40*, 501–509; b) C. D. Brown, M. L. Neidig, M. B. Neibergall, J. D. Lipscomb, E. I. Solomon, *J. Am. Chem. Soc.* **2007**, *129*, 7427–7438.
[15] S. Aluri, S. P. de Visser, *J. Am. Chem. Soc.* **2007**, *129*, 14846–14847.
[16] E. P. Tchesnokov, A. S. Faponle, C. G. Davies, M. G. Quesne, R. Turner, M. Fellner, R. J. Souness, S. M. Wilbanks, S. P. de Visser, G. N. L. Jameson, *Chem. Commun.* **2016**, *52*, 8814–8817.
[17] J. Shearer, R. C. Scarrow, J. A. Kovacs, *J. Am. Chem. Soc.* **2002**, *124*, 11709–11717.
[18] J. A. Kovacs, *Chem. Rev.* **2004**, *104*, 825–848.
[19] T. Kitagawa, A. Dey, P. Lugo-Mas, J. B. Benedict, W. Kaminsky, E. Solomon, J. A. Kovacs, *J. Am. Chem. Soc.* **2006**, *128*, 14448–14449.

[20] L. Wang, M. Gennari, F. G. Cantú Reinhard, J. Gutiérrez, A. Morozan, C. Philouze, S. Demeshko, V. Artero, F. Meyer, S. P. de Visser, et al., *J. Am. Chem. Soc.* **2019**, *141*, 8244–8253.

[21] T. Ohta, T. Tachiyama, K. Yoshizawa, T. Yamabe, T. Uchida, T. Kitagawa, *Inorg. Chem.* **2000**, *39*, 4358–4369.

[22] M. Gennari, C. Duboc, *Acc. Chem. Res.* **2020**, *53*, 2753–2761.

[23] G. Moula, J. Bag, M. Bose, S. Barman, K. Pal, *Inorg. Chem.* **2022**, *61*, 6660–6671.

[24] M. K. Coggins, X. Sun, Y. Kwak, E. I. Solomon, E. Rybak-Akimova, J. A. Kovacs, *J. Am. Chem. Soc.* **2013**, *135*, 5631–5640.

[25] M. Gennari, D. Brazzolotto, J. Pécaut, M. V. Cherrier, C. J. Pollock, S. DeBeer, M. Retegan, D. A. Pantazis, F. Neese, M. Rouzières, et al., *J. Am. Chem. Soc.* **2015**, *137*, 8644–8653.

[26] a) J. A. Kovacs, *Acc. Chem. Res.* **2015**, *48*, 2744–2753; b) P. Kumar, L. Devkota, M. C. Casey, A. A. Fischer, S. V. Lindeman, A. T. Fiedler, *Inorg. Chem.* **2022**, *61*, 16664–16677.

[27] P. Gerschel, B. Battistella, D. Siegmund, K. Ray, U.-P. Apfel, *Organometallics* **2020**, *39*, 1497–1510.

[28] L. Iffland, D. Siegmund, U.-P. Apfel, *Z. Anorg. Allg. Chem.* **2020**, *646*, 746–753.

[29] D. Hamdane, H. Zhang, P. Hollenberg, *Photosynth. Res.* **2008**, *98*, 657.

[30] a) C. W. Anson, S. S. Stahl, *Chem. Rev.* **2020**, *120*, 3749–3786; b) J. Rosenthal, D. G. Nocera, *Acc. Chem. Res.* **2007**, *40*, 543–553; c) W. Zhang, W. Lai, R. Cao, *Chem. Rev.* **2017**, *117*, 3717–3797; d) M. L. Pegis, C. F. Wise, D. J. Martin, J. M. Mayer, *Chem. Rev.* **2018**, *118*, 2340–2391; e) D. Das, Y.-M. Lee, K. Ohkubo, W. Nam, K. D. Karlin, S. Fukuzumi, *J. Am. Chem. Soc.* **2013**, *135*, 2825; f) S. Fukuzumi, S. Mandal, K. Mase, K. Ohkubo, H. Park, J. Benet-Buchholz, W. Nam, A. Llobet, *J. Am. Chem. Soc.* **2012**, *134*, 9906; g) D. Das, Y.-M. Lee, K. Ohkubo, W. Nam, K. D. Karlin, S. Fukuzumi, *J. Am. Chem. Soc.* **2013**, *135*, 4018; h) C. Costentin, H. Dridi, J.-M. Saveant, *J. Am. Chem. Soc.* **2015**, *137*, 13535; i) F. Heims, K. Ray, M. Schwalbe, W. Nam, *Curr. Opin. Chem. Biol.* **2015**, *25*, 159–171; j) S. Bhunia, A. Ghatak, A. Dey, *Chem. Rev.* **2022**, *122*, 12370–12426.

[31] a) M. Guo, T. Corona, K. Ray, W. Nam, *ACS Cent. Sci.* **2019**, *5*, 13–28; b) X.-P. Zhang, A. Chandra, Y.-M. Lee, R. Cao, K. Ray, W. Nam, *Chem. Soc. Rev.* **2021**, *50*, 4804–4811; c) K. Ray, F. F. Pfaff, B. Wang, W. Nam, *J. Am. Chem. Soc.* **2014**, *136*, 13942–13958.

[32] Y.-H. Wang, B. Mondal, S. S. Stahl, *ACS Catal.* **2020**, *10*, 12031–12039.

[33] A. Paul, R. Borrelli, H. Bouyanfif, S. Gottis, F. Sauvage, *ACS Omega* **2019**, *4*, 14780–14789.

[34] I. Monte-Pérez, S. Kundu, A. Chandra, K. E. Craigo, P. Chernev, U. Kuhlmann, H. Dau, P. Hildebrandt, C. Greco, C. Van Stappen, et al., *J. Am. Chem. Soc.* **2017**, *139*, 15033–15042.

[35] J. P. Hurvois, C. Moinet, *J. Organomet. Chem.* **2005**, *690*, 1829–1839.

[36] The ferrocenium (Fc^+) cation is known to be unstable in acidic environment in presence of dioxygen; therefore Fc* was used as electron donor due to the higher stability of the decamethylferrocenium (Fc^{*+}) cation.

[37] N. A. Stephenson, A. T. Bell, *Anal. Bioanal. Chem.* **2005**, *381*, 1289–1293.

[38] Y.-H. Wang, M. L. Pegis, J. M. Mayer, S. S. Stahl, *J. Am. Chem. Soc.* **2017**, *139*, 16458–16461.

[39] Y.-H. Wang, Z. K. Goldsmith, P. E. Schneider, C. W. Anson, J. B. Gerken, S. Ghosh, S. Hammes-Schiffer, S. S. Stahl, *J. Am. Chem. Soc.* **2018**, *140*, 10890–10899.

[40] a) J. B. Gordon, A. C. Vilbert, M. A. Siegler, K. M. Lancaster, P. Moënne-Loccoz, D. P. Goldberg, *J. Am. Chem. Soc.* **2019**, *141*, 3641–3653; b) A. A. Fischer, S. V. Lindeman, A. T. Fiedler, *Dalton Trans.* **2017**, *46*, 13229–13241.

[41] T. Corona, S. K. Padamati, F. Acuña-Parés, C. Duboc, W. R. Browne, A. Company, *Chem. Commun.* **2017**, *53*, 11782–11785.

[42] B. Lv, X. Li, K. Guo, J. Ma, Y. Wang, H. Lei, F. Wang, X. Jin, Q. Zhang, W. Zhang, et al., *Angew. Chem. Int. Ed.* **2021**, *60*, 12742–12746; *Angew. Chem.* **2021**, *133*, 12852–12856.

[43] K. Mittra, B. Mondal, A. Mahammed, Z. Gross, A. Dey, *Chem. Commun.* **2017**, *53*, 877–880.

[44] M. A. Dedushko, D. Schweitzer, M. N. Blakely, R. D. Swartz, W. Kaminsky, J. A. Kovacs, *J. Biol. Inorg. Chem.* **2019**, *24*, 919–926.

[45] C.-L. Wong, J. A. Switzer, K. P. Balakrishnan, J. F. Endicott, *J. Am. Chem. Soc.* **1980**, *102*, 5511–5518.

[46] C.-L. Wong, J. F. Endicott, *Inorg. Chem.* **1981**, *20*, 2233–2239.

[47] K. Kumar, J. F. Endicott, *Inorg. Chem.* **1984**, *23*, 2447–2452.

[48] a) A. Bakac, J. H. Espenson, *J. Am. Chem. Soc.* **1990**, *112*, 2273–2278; b) H. Kim, P. J. Rogler, S. K. Sharma, A. W. Schaefer, E. I. Solomon, K. D. Karlin, *J. Am. Chem. Soc.* **2020**, *142*, 3104–3116; c) J. J. D. Sacramento, T. Albert, M. Siegler, P. Moënne-Loccoz, D. P. Goldberg, *Angew. Chem. Int. Ed.* **2022**, *61*, e202111492; *Angew. Chem.* **2022**, *134*, e202111492.

[49] C.-C. Wang, H.-C. Chang, Y.-C. Lai, H. Fang, C.-C. Li, H.-K. Hsu, Z.-Y. Li, T.-S. Lin, T.-S. Kuo, F. Neese, et al., *J. Am. Chem. Soc.* **2016**, *138*, 14186–14189.

[50] a) A. R. Corcos, O. Villanueva, R. C. Walroth, S. K. Sharma, J. Bacsa, K. M. Lancaster, C. E. MacBeth, J. F. Berry, *J. Am. Chem. Soc.* **2016**, *138*, 1796–1799; b) J. Cho, R. Sarangi, H. Y. Kang, J. Y. Lee, M. Kubo, T. Ogura, E. I. Solomon, W. Nam, *J. Am. Chem. Soc.* **2010**, *132*, 47, 16977–16986; c) Y. Jo, J. Annaraj, M. S. Seo, Y.-M. Lee, S. Y. Kim, J. Cho, W. Nam, *J. Inorg. Biochem.* **2008**, *102*, 2155–2159.

[51] a) A. Brinkmeier, R. A. Schulz, M. Buchhorn, C.-J. Spyra, S. Dechert, S. Demeshko, V. Krewald, F. Meyer, *J. Am. Chem. Soc.* **2021**, *143*, 10361–10366.

[52] Calculations on **2a** were performed for the different possible spin states ($S=5/2$, 3/2, and 1/2) and orientations (*cis* and *trans*). The calculated energies are summarized in Table S4 (bottom) and the optimized structure in the EPR determined $S=3/2$ state for **2a** in *trans* configuration is shown in Figure S24f. The $S=5/2$ state lies very high in energy and can be excluded. Although, the $S=3/2$ and $S=1/2$ states of **2a** are isoenergetic within the error of the DFT calculated energies (typically 5 kcal mol^{-1}), its EPR spectrum clearly identifies a high-spin $S=3/2$ state. DFT calculations also cannot distinguish between the two possible isomers (*cis* and *trans*) based on calculated energies; however, the fine structure pattern in the EXAFS waves and the corresponding Fourier Transform clearly favor the predominant formation of the trans isomer (Figure S23). Notably, the *trans* configuration is also visible in the XRD structures of **2** (ref. [28]) and **2b**. The alternate assignment of $S=3/2$ **2a** containing a high spin ($S=2$) Co^{III} center antiferromagnetically coupled to $S=1/2$ dithiacyclam-$O_2^{\bullet-}$ unit is excluded considering the rarity of octahedral high-spin Co^{III} centers (a) H. C. Clark, B. Cox, A. G. Sharpe, *J. Chem. Soc.* **1957**, 4132–4133; b) P. Guetlich, B. R. McGarvey, W. Klaeui, *Inorg. Chem.* **1980**, *19*, 3704–3706.) and based on the observed low-spin $S=1/2$ ground state for the Co^{II} centre in **2**.

[53] Deposition Number 2193635 contains the supplementary crystallographic data for this paper. These data are provided free of charge by the joint Cambridge Crystallographic Data Centre and Fachinformationszentrum Karlsruhe Access Structures service.

Manuscript received: September 23, 2022
Accepted manuscript online: November 15, 2022
Version of record online: December 29, 2022